Stability of laminar viscoplastic flows down an inclined open channel

Stability of laminar viscoplastic flows down an inclined open channel

Lorenzo Fusi, Benedetta Calusi, Angiolo Farina, Fabio Rosso

Dipartimento di Matematica e Informatica "Ulisse Dini", Viale Morgagni 67/a, 50134 Firenze

Abstract

In this paper we study the two-dimensional linear stability of a Papanastasiou fluid flowing down an inclined plane. The Papanastasiou constitutive law is a regularization of the Bingham law in which the singularity at zero strain rate is smoothed by an exponential function.

The stability eigenvalue problem is solved by a spectral collocation method based on Chebyshev polynomials. We prove that, while the Bingham flow is unconditionally stable for every Reynolds number, the Papanastasiou flow becomes unstable at a critical Reynolds that depends on the material parameters, on the angle of inclination of the plane and on the prescribed inlet discharge. In particular, we show that the critical Reynolds is a decreasing function of the yield stress, showing the destabilizing effect of the yield stress. The results obtained here show that the stability characteristics of a regularized flow can be extremely different from that of the exact Bingham fluid even if the two flows are "practically indistinguishable".

Keywords: Bingham fluid, Papanastasiou fluid, linear stability, free surface flow

[*] Fully documented templates are available in the elsarticle package on CTAN.
[1] Since 1880.

1. Introduction

Viscoplastic materials are characterized by the presence of a yield stress below which deformations are not possible. Below the yield stress the fluid behaves like a rigid body and above the yield stress the material behaves as a fluid. When the constitutive response above the yield stress is linear we have the so-called Bingham fluid. When the response is nonlinear we have a series of viscoplastic models, such as the Herschel-Bulkley fluid or the Casson fluid, depending on the type of nonlinearity.

Viscosity regularization methods are probably the most popular methods for studying viscoplastic flows. As a matter of fact, regularized constitutive equations allow one to get rid of the issues caused by the inherent singularity that characterizes viscoplastic models, [16]. In regularized models the yield surface separating the yielded zone from the unyielded zone is approximated by setting the level set of the norm of the stress equal to the yield stress. Contrary to exact viscoplastic models, in approximated models the stress is indeed defined everywhere and the local form of the momentum equation holds everywhere in the fluid domain.

Regularized constitutive equations are characterized by a parameter that controls the level of approximation. When such a parameter tends to a specific value (typically 0 or ∞), the approximated model converges to the exact one, [7]. Of course, the selection of the regularized law is arbitrary and different choices are possible.

Despite all the advantages coming from the usage of regularized models, there are situations in which some physical properties of the viscoplastic fluid are not recovered when the approximated model tends to the exact one. Some interesting examples of this paradoxical behavior are presented in [13], where it is shown, for instance, that in lubrication and thin film flows the regularization error in the detection of the yield surface can be pretty large. Recently in [15] it was shown that, when using a regularized constitutive law (see [21]) to investigate the response to disturbances in a Plane Poiseuille Bingham flow, the stability characteristics predicted by the use of viscosity regularization are different from the ones obtained using the exact Bingham model.

All these results seem to indicate that one should be very careful when using exact viscoplastic models to predict flow properties, since in some cases some of these properties are not retrieved from the approximated models (see [1], [3] for a discussion on the the real existence of the yield stress). One must bear in mind that truly undeformable materials do not exist in real life and all materials are deformable to a certain degree. We refer the reader to the paper [3] for an interesting discussion on the real existence of the yield-stress from the experimental and theoretical point of view. Therefore, if a property is not recovered from a regularized fluid whose response is "practically identical" to that of a viscoplastic fluid, maybe the correct property is that of the regularized fluid and not vice versa. We are not stating that viscoplastic models are useless - see for instance [14] where the authors discuss the utility of the Bingham model in Oil and Gas industry - we are just saying that one must be very careful because the characteristics of certain flows predicted by the exact models are not recovered from the regularized ones and discrepancies may arise between the regularized and the exact models.

In this paper we study the linear stability of a Papanastasiou fluid flowing down an incline with no surface tension. The Papanastasiou model is a regularization of the Bingham model in which the singularity at zero strain rate is smoothed by an exponential function, see [21]. We shall show that the stability properties are completely different from those of a Bingham fluid and that, while the Bingham flow is unconditionally stable for every Reynolds number and for every angle of inclination in agreement with [11], the Papanastasiou flow exhibits surface modes that may become unstable above a critical Reynolds number (which is a decreasing function of the angle of inclination). The discrepancy between the Bingham and the Papanastasiou model here is even more evident than in the plane Poiseuille flow, see [15]. Indeed, in the latter case it was proved that the regularized flow was more stable than the Bingham flow with a discrepancy in the critical Reynolds numbers of the order of ten. In such situation the qualitative behavior of the two flows was different but "not extremely different". Here, the situation is more drastic since the Bingham flow is always stable, while the approximated flow can be extremely unstable. We shall also see that the Papanastasiou flow is less stable than the Newtonian flow, proving that the presence of the "yield stress" has a destabilizing effect. This result is in contrast with that of channel flow where the yield stress tends to stabilize the flow, see [13].

The paper is organized as follows: in Section 2 we derive the governing equations and the basic dimensionless Bingham and Papanastasiou primary flow. In Section 3 we perform a linear temporal stability analysis and we formulate the eigenvalue problem that governs the evolution of the disturbances. In Section 4 we solve the eigenvalue problem numerically using a spectral collocation method. The results obtained in the Bingham and Papanastasiou cases are discussed in Section 5. The final section is devoted to conclusions.

2. The Mathematical model

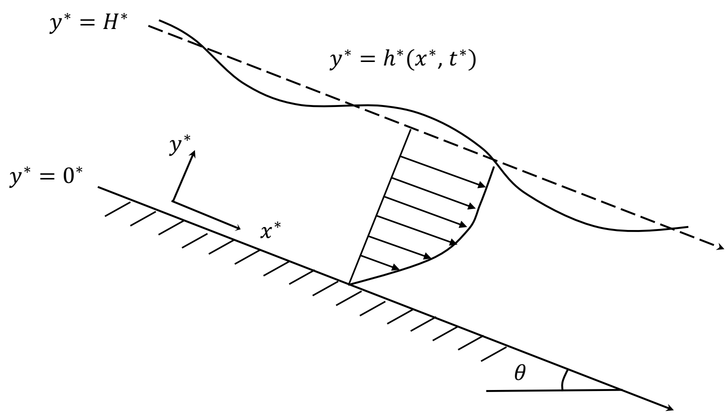

Figure 1: Sketch of the system.

We consider the flow of an incompressible fluid flowing down an inclined plane as depicted in Fig. 1. The two-dimensional fluid velocity is

$$\mathbf{v}^*(x^*, y^*, t^*) = u^*(x^*, y^*, t^*)\mathbf{i} + v^*(x^*, y^*, t^*)\mathbf{j}.$$

Because of incompressibility we decompose the constitutive law as

$$\mathbf{T}^* = -p^*\mathbf{I} + \mathbf{S}^*,$$

where p^* is the pressure and $\mathbf{S}^*$ is the deviatoric part of the Cauchy stress. Newtonian fluids are such that $\mathbf{S}^* = 2\mu^*\mathbf{D}^*$, μ^* being the viscosity and $\mathbf{D}^*$ the symmetric part of the velocity gradient. The Bingham law is formulated mathematically as follows

$$\begin{cases} \mathbf{S}^* = \left[2\mu^* + \dfrac{\tau_o^*}{|\mathbf{D}^*|}\right]\mathbf{D}^*, & |\mathbf{S}^*| \geqslant \tau_o^*, \\ \\ \mathbf{D}^* = 0, & |\mathbf{S}^*| \leqslant \tau_o^*, \end{cases} \tag{1}$$

where

$$|\mathbf{D}^*| = \sqrt{\frac{1}{2}\mathbf{D}^* \cdot \mathbf{D}^*}, \qquad |\mathbf{S}^*| = \sqrt{\frac{1}{2}\mathbf{S}^* \cdot \mathbf{S}^*},$$

and where τ_o^* is the yield stress. Model (1) can be approximated by the following law (see [21])

$$\mathbf{S}^* = \left[2\mu^* + \frac{\tau_o^*\left(1 - \exp(-\frac{|\mathbf{D}^*|}{\epsilon^*})\right)}{|\mathbf{D}^*|}\right]\mathbf{D}^*, \tag{2}$$

where ϵ^* is a parameter with the dimension of a strain rate. When $\epsilon^* \to 0$ the Bingham model is formally recovered, while for $\epsilon^* \to \infty$ we retrieve the Newtonian law. A quantitative analysis of the convergence of the Papanastasiou model to the Bingham model is presented in [15]. The equations governing the flow are

$$\begin{cases} \rho^* \dfrac{d\mathbf{v}^*}{dt^*} = -\nabla^* p^* + \nabla^* \cdot \mathbf{S}^* + \rho^* g^* \Big(\sin\theta\mathbf{i} - \cos\theta\mathbf{j}\Big), \\ \\ \nabla^* \cdot \mathbf{v}^* = 0, \end{cases} \tag{3}$$

where ρ^* is the constant density, g^* is gravity and θ is the tilt angle. If we neglect the effect of surface tension, the boundary conditions at the free surface

$y^* = h^*(x^*, t^*)$ are

$$\begin{cases} \dfrac{\partial h^*}{\partial t^*} + u^* \dfrac{\partial h^*}{\partial x^*} = v^*, & y^* = h^*, \\[2em] \left(\dfrac{\partial h^*}{\partial x^*}\right)^2 (p^* - S^*_{11}) + 2\left(\dfrac{\partial h^*}{\partial x^*}\right) S^*_{12} + (p^* - S^*_{22}) = 0, & y^* = h^*, \\[2em] S^*_{12}\left[\left(\dfrac{\partial h^*}{\partial x^*}\right)^2 - 1\right] + \dfrac{\partial h^*}{\partial x^*}(S^*_{11} - S^*_{22}) = 0, & y^* = h^*. \end{cases} \tag{4}$$

The first equation in (4) is the kinematic condition while $(4)_{2,3}$ express the absence of normal and tangential stress on the free surface. On the bottom plane we take the impermeability no-slip condition $\mathbf{v}^*(0) = 0$. We non-dimensionalize the problem employing the following transformation

$$\mathbf{x}^* = H^*\mathbf{x}, \qquad t^* = \left(\frac{H^*}{U^*}\right) t, \qquad \mathbf{v}^* = U^*\mathbf{v}, \qquad p^* = \left(\frac{\mu^* U^*}{H^*}\right) p, \tag{5}$$

$$\mathbf{S}^* = \left(\frac{\mu^* U^*}{H^*}\right)\mathbf{S}, \qquad \mathbf{D}^* = \left(\frac{U^*}{H^*}\right)\mathbf{D}, \quad h^* = H^* h, \tag{6}$$

where H^* is the characteristic height of the fluid layer (which depends on the prescribed inlet discharge) and U^* is a characteristic velocity yet to be determined. The dimensionless constitutive law of the Bingham fluid becomes

$$\begin{cases} \mathbf{S} = \left[2 + \dfrac{B}{|\mathbf{D}|}\right]\mathbf{D}, & |\mathbf{S}| \geqslant B, \\[2em] \mathbf{D} = 0, & |\mathbf{S}| \leqslant B, \end{cases} \tag{7}$$

where

$$B = \left(\frac{\tau_o^* H^*}{\mu^* U^*}\right), \tag{8}$$

is the Bingham number. The dimensionless Papanastasiou law is

$$\mathbf{S} = \left[2 + \frac{B\left(1 - \exp(-\frac{2|\mathbf{D}|}{\epsilon})\right)}{|\mathbf{D}|}\right]\mathbf{D}, \tag{9}$$

where

$$\epsilon = \left(\frac{2\epsilon^* H^*}{U^*}\right),$$

is a parameter that defines the degree of approximation. Equations (3) become

$$\begin{cases} Re\,\dfrac{d\mathbf{v}}{dt} = -\nabla p + \nabla\cdot\mathbf{S} + \dfrac{Re}{Fr^2}\Big(\sin\theta\mathbf{i} - \cos\theta\mathbf{j}\Big), \\ \\ \nabla\cdot\mathbf{v} = 0. \end{cases} \tag{10}$$

where

$$Re = \left(\frac{\rho^* U^* H^*}{\mu^*}\right), \qquad Fr^2 = \left(\frac{{U^*}^2}{g^* H^*}\right), \tag{11}$$

are the Reynolds number and squared Froude number respectively. The dimensionless boundary conditions are

$$\begin{cases} \mathbf{v} = 0, & y = 0, \\ \\ \dfrac{\partial h}{\partial t} + u\dfrac{\partial h}{\partial x} = v, & y = h, \\ \\ \left(\dfrac{\partial h}{\partial x}\right)^2 (p - S_{11}) + 2\left(\dfrac{\partial h}{\partial x}\right) S_{12} + (p - S_{22}) = 0, & y = h, \\ \\ S_{12}\left[\left(\dfrac{\partial h}{\partial x}\right)^2 - 1\right] + \dfrac{\partial h}{\partial x}(S_{11} - S_{22}) = 0, & y = h. \end{cases} \tag{12}$$

We look for a basic primary flow $\mathbf{v} = u(y)\mathbf{i}$, $h = 1$ (notice that in this case mass balance is automatically satisfied). The momentum equation is reduced to

$$\begin{cases} 0 = -\dfrac{\partial p}{\partial x} + \dfrac{\partial S_{12}}{\partial y} + \xi, \\ \\ 0 = -\dfrac{\partial p}{\partial y} - \xi\cot\theta, \end{cases} \qquad \xi = \frac{Re}{Fr^2}\sin\theta, \tag{13}$$

where $S_{12} = S_{12}(y)$ is the only non zero component of the tensor $\mathbf{S}$. In this case the boundary conditions on $y = 1$ are reduced to $p = S_{12} = 0$. Hence, integration of the momentum equations yields

$$p = \xi\cot\theta\big(1 - y\big), \qquad S_{12} = \xi\sin\theta\big(1 - y\big). \tag{14}$$

Note that $2|\mathbf{D}| = u'$, where $(\cdot)'$ stands for differentiation with respect to y. We see that

$$\xi = \frac{\rho^* g^* {H^*}^2 \sin\theta}{\mu^* U^*} = \frac{{\rho^*}^2 {H^*}^3 g^* \sin\theta}{{\mu^*}^2 Re},$$

so that

$$H^* = \left[\frac{{\mu^*}^2 \xi Re}{{\rho^*}^2 g^* \sin\theta}\right]^{1/3}.$$

As a consequence

$$B = \frac{\tau_o^* H^*}{\mu^* U^*} = \frac{\tau_o^* \rho^* {H^*}^2}{{\mu^*}^2 Re} = \underbrace{\left[\frac{{\tau_o^*}^3}{{\mu^*}^2 {g^*}^2 \rho^* \sin^2\theta}\right]^{1/3}}_{\Gamma} \frac{\xi^{2/3}}{Re^{1/3}} = \frac{\Gamma \xi^{2/3}}{Re^{1/3}}. \tag{15}$$

We write

$$\Gamma = \frac{\gamma}{\sqrt[3]{\sin^2\theta}}, \qquad \gamma = \frac{\tau_o^*}{\left[{\mu^*}^2 {g^*}^2 \rho^*\right]^{1/3}} \tag{16}$$

so that γ is a non-dimensional parameter that depends only on the material properties of the fluid, while Γ depends also on the tilt angle θ. We observe that the Bingham number is a flow-dependent quantity and that, at this stage, the characteristic velocity U^* is yet to be defined. We see that Γ can be interpreted as a "yield-stress" number or, in other words, as a Bingham number independent of the flow. In the linear stability analysis presented in Section 3, where Re is increased to determine the critical conditions, we shall consider Γ (and not B) as a fixed material number, since Γ does not depend on Re.

Now we proceed considering the Bingham problem and the Papanastasiou problem.

2.1. Bingham basic profile

When employing the Bingham model equation (13) yields

$$\left(u' + B\right)' = -\xi, \qquad \xi = \frac{Re}{Fr^2}\sin\theta, \tag{17}$$

which holds only in the fluid domain $[0,\sigma]$, $y=\sigma$ being the yield surface. On the yield surface $S_{12} = B$ and hence $u' = 0$. Therefore, integrating (17) twice with $u'(\sigma) = 0$ and $u(0) = 0$, we get

$$u(y) = \xi\left[\frac{\sigma^2}{2} - \frac{(\sigma - y)^2}{2}\right], \qquad y \in [0,\sigma]. \tag{18}$$

The momentum balance of the rigid part lying above the yield surface is

$$\sigma = 1 - \frac{\tau_o^*}{\rho^* g^* H^* \sin\theta} = 1 - \frac{B}{\xi}, \tag{19}$$

so that the yielded part is present (and the motion is possible) only if $\xi > B$, i.e. if

$$\rho^* g^* H^* \sin\theta > \tau_o^*.$$

Now, we select the characteristic velocity U^* so that $u(\sigma) = 1$. This implies $\xi\sigma^2 = 2$, i.e.

$$2 = \xi\left(1 - \frac{B}{\xi}\right)^2 \qquad \Longrightarrow \qquad \xi^2 - 2(B+1)\xi + B^2 = 0.$$

The only acceptable solution of the algebraic equation above is

$$\xi = B + 1 + \sqrt{2B+1} > B. \tag{20}$$

In conclusion the normalized profile $u(y)$ is given by

$$u(y) = \begin{cases} 1 - \left(1 - \dfrac{y}{\sigma}\right)^2, & y \in [0, \sigma], \\ \\ 1, & y \in [\sigma, 1], \end{cases} \tag{21}$$

with

$$\sigma = \left[\frac{1 + \sqrt{2B+1}}{1 + B + \sqrt{2B+1}}\right] < 1. \tag{22}$$

We recall that B is given by (15), so that on eliminating ξ from (15) and (20) we get

$$B = \frac{\Gamma\left[B + 1 + \sqrt{2B+1}\right]^{2/3}}{Re^{1/3}}. \tag{23}$$

Equation (23) provides the relation between B and Re for each Γ. The plot of the function $B(Re)$ is shown in Fig. 2.

2.2. Papanastasiou profile

When employing the Papanastasiou model we get

$$S_{12} = u' + B\left[1 - \exp\left(-\frac{u'}{\epsilon}\right)\right] = \frac{Re}{Fr^2}\sin\theta(1-y). \tag{24}$$

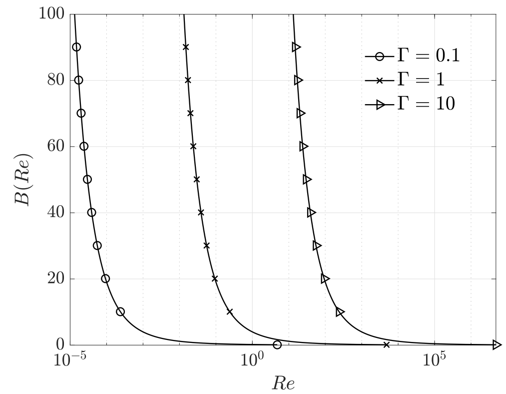

Figure 2: Plot of $B = B(Re)$ in the Bingham case for different values of Γ.

Equation (24) can be solved with respect to u' using the Lambert function $\mathcal{W}$, see [25]. We obtain

$$u' = \xi\big(1-y\big) - B + \epsilon\mathcal{W}\left[\frac{B}{\epsilon}\exp\left(\frac{B+\xi(y-1)}{\epsilon}\right)\right], \qquad \xi = \frac{Re}{Fr^2}\sin\theta. \quad (25)$$

Integrating the above between 0 and y and exploiting the no-slip condition, we find

$$u(y) = \xi\left[y - \frac{y^2}{2}\right] - By + \epsilon\int_0^y \mathcal{W}\left[\frac{B}{\epsilon}\exp\left(\frac{B+\xi(\eta-1)}{\epsilon}\right)\right]d\eta. \quad (26)$$

Using the transformation

$$z = \frac{B}{\epsilon}\exp\left(\frac{B+\xi(\eta-1)}{\epsilon}\right), \qquad d\eta = \frac{\epsilon}{\xi}\frac{dz}{z}, \quad (27)$$

we obtain

$$u(y) = \xi\left[y - \frac{y^2}{2}\right] - By + \frac{\epsilon^2}{\xi}\int_{\frac{B}{\epsilon}e^{\left(\frac{B-\xi}{\epsilon}\right)}}^{\frac{B}{\epsilon}e^{\left(\frac{B+\xi(y-1)}{\epsilon}\right)}} \frac{\mathcal{W}(z)}{z}dz. \quad (28)$$

From classical results on the Lambert function ([25]) we know that

$$\int\frac{\mathcal{W}(z)}{z}dz = \frac{\mathcal{W}(z)^2}{2} + \mathcal{W}(z) + const,$$

so that

$$u(y) = \xi\left[y - \frac{y^2}{2}\right] - By + \frac{\epsilon^2}{2\xi}\Big[\mathcal{W}(z)^2 + 2\mathcal{W}(z)\Big]_{\frac{B}{\epsilon}e^{\left(\frac{B-\xi}{\epsilon}\right)}}^{\frac{B}{\epsilon}e^{\left(\frac{B+\xi(y-1)}{\epsilon}\right)}}. \quad (29)$$

We normalize the velocity of the free surface so that $u(1) = 1$, namely

$$1 = \frac{\xi}{2} - B + \frac{\epsilon^2}{2\xi}\Big[\mathcal{W}(z)^2 + 2\mathcal{W}(z)\Big]_{\frac{B}{\epsilon}e^{\left(\frac{B-\xi}{\epsilon}\right)}}^{\frac{B}{\epsilon}e^{\left(\frac{B}{\epsilon}\right)}}. \tag{30}$$

Recalling (15), relation (30) can be rewritten as

$$1 = \frac{\xi}{2} - \frac{\Gamma\xi^{2/3}}{Re^{1/3}} + \frac{\epsilon^2}{2\xi}\Big[\mathcal{W}(z)^2 + 2\mathcal{W}(z)\Big]_{\frac{\Gamma\xi^{2/3}}{Re^{1/3}\epsilon}e^{\left(\frac{\Gamma\xi^{2/3}}{Re^{1/3}\epsilon}-\frac{\xi}{\epsilon}\right)}}^{\frac{\Gamma\xi^{2/3}}{Re^{1/3}\epsilon}e^{\left(\frac{\Gamma\xi^{2/3}}{Re^{1/3}\epsilon}\right)}}. \tag{31}$$

Relation (31) provides the link between ξ and Re, i.e. the function $\xi = \xi(Re)$

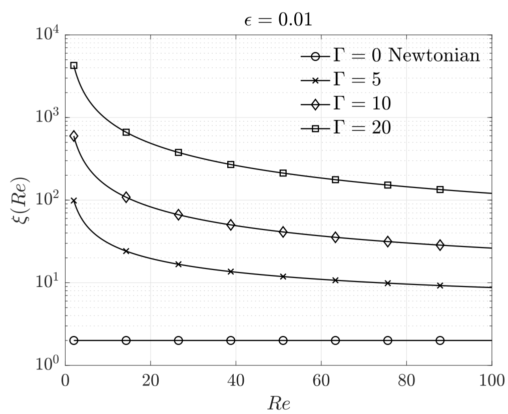

Figure 3: Plot of $\xi = \xi(Re)$ in the Papanastasiou case for different values of Γ.

for given Γ and ϵ. For every positive Re, it is always possible to determine ξ satisfying (31). The function $\xi = \xi(Re)$ for $\epsilon = 0.01$ and various Γ is shown in Fig. 3, from which it is evident that ξ is a decreasing function of Re. It is interesting to notice that when $\Gamma = 0$ (Newtonian fluid) we get $\xi \equiv 2$ independently of Re, and in this case the velocity profile is

$$u(y) = 2y - y^2.$$

If we couple equations (29) and (30), we can write the basic Papanastasiou flow as

$$u(y) = 1 + \xi\left(y - \frac{y^2}{2} - \frac{1}{2}\right) + B(1-y) +$$

$$\frac{\epsilon^2}{2\xi}\left[\left(\mathcal{W}^2 + 2\mathcal{W}\right)\Big|_{\frac{B}{\epsilon}e^{\left(\frac{B-\xi(1-y)}{\epsilon}\right)}} - \frac{B}{\epsilon}\left(\frac{B}{\epsilon} + 2\right)\right], \tag{32}$$

where

$$\xi = \xi(Re), \qquad B = \frac{\Gamma\left[\xi(Re)\right]^{2/3}}{Re^{1/3}}.$$

Therefore, the velocity profile of the Papanastasiou fluid depends only on Re and on the parameters Γ and ϵ. Now, we can use (21) and (32) to adjust the parameter ϵ so that the Papanastasiou velocity profile represents a good approximation of the Bingham profile. We shall see that $\epsilon = 0.01$ is a good choice for almost every Γ. We define the relative error (in percentage) between the Bingham and Papanastasiou profile as

$$E_r = 100 \times \max\left|1 - \frac{u_P(y)}{u_B(y)}\right|, \tag{33}$$

where $u_B(y)$ is the Bingham velocity given by (21) and $u_P(y)$ is the Papanastasiou velocity given by (32). In Fig. 4 we plot the relative error (33) as a function of ϵ for $Re = 5$ and for $\Gamma = 0.1, 1, 5, 15$. As one can see, for the selected range of Γ, a good choice of ϵ is any value between 10^{-3} and 10^{-2}, which provides a relative error less than 0.3%. In Fig. 5, we plot the relative error (33) for $\Gamma = 5$

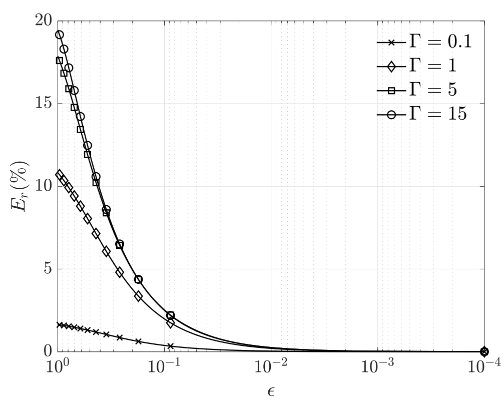

Figure 4: Relative error (33) as a function of ϵ for $Re = 5$ and $\Gamma = 0.1, 1, 5, 15$.

and $Re = 5, 50, 200, 1000$. Once again we notice that $\epsilon = 0.01$ is a choice that guarantees that $E_r < 0.5\%$. The dimensional discharge across a section is given by

$$Q^* = U^* H^* \int_0^1 u(y; \Gamma, Re, \epsilon)dy. \tag{34}$$

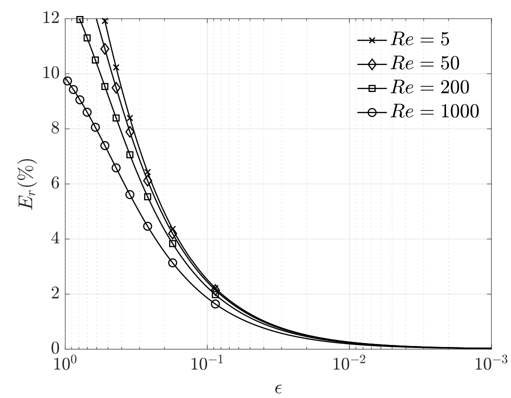

Figure 5: Relative error (33) as a function of ϵ for $\Gamma = 5$ and $Re = 5, 50, 200, 1000$.

If we rescale Q^* with μ^*/ρ^* we get

$$Q = Re \int_0^1 u(y; \Gamma, Re, \epsilon) dy. \tag{35}$$

For given Γ and ϵ the relation (35) provides the link between the dimensionless discharge and the Reynolds number. In Fig. 6 we display the discharge Q as a monotone function of Re for $\epsilon = 0.01$ and $\Gamma = 0, 5, 15, 30, 50$. As physically expected, the function $Q(Re)$ is monotonically increasing with Re. We notice also that the relation is almost linear.

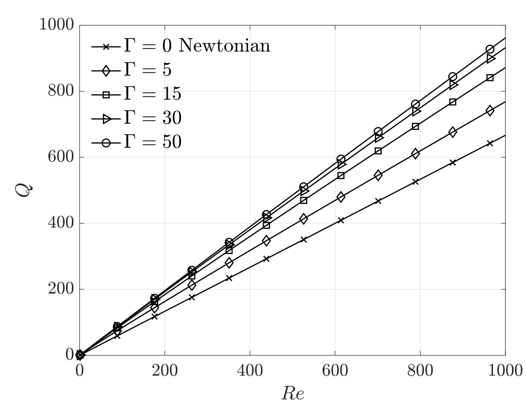

Figure 6: Discharge $Q = Q(Re)$ given by (35) for $\Gamma = 0, 5, 15, 30, 50$ and $\epsilon = 0.01$.

Table 1: Material parameters and coefficient γ given by (16).

Reference	Material	τ_o^* (Pa)	μ^* (Pa$\cdot$ sec)	ρ^* (Kg/m^3)	γ
[20]	Mud	3	5	1200	0.0211
[23]	Carbopol slurry	17	0.43	1000	0.641
[23]	Kaoline slurry	0.875	0.034	1450	0.0161

In Table 1 we report some typical values of the rheological parameters and the corresponding value of γ given by (16) taken from the literature. For most practical application the parameter γ ranges between 10^{-2} and 1.

3. Linear stability analysis

In this section we perform a linear stability analysis to detect how the primary flows (Bingham and Papanastasiou) respond to small disturbances. We consider an infinitesimal perturbation of the basic flow (u_b, p_b), where the subscript $(\cdot)_b$ is used to denote the basic solutions determined in the previous section. In particular p_b comes from $(14)_1$ and u_b is the velocity (21) (Bingham) or (32) (Papanastasiou). We perform a two-dimensional temporal linear stability study of the problem in which the perturbed solution is sought in the form

$$\begin{cases} u = u_b(y) + \hat{u}(y)e^{i\alpha(x-ct)}, \\ \\ v = \hat{v}(y)e^{i\alpha(x-ct)}, \\ \\ p = p_b(y) + \hat{p}(y)e^{i\alpha(x-ct)}. \end{cases} \qquad \Longrightarrow \qquad \begin{cases} \mathbf{S} = \mathbf{S}_b(y) + \hat{\mathbf{S}}(y)e^{i\alpha(x-ct)}, \\ \\ \mathbf{D} = \mathbf{D}_b + \hat{\mathbf{D}}(y)e^{i\alpha(x-ct)}, \end{cases} \tag{36}$$

where $\alpha \in \mathbb{R}$ is the wavenumber and $c = c_r + ic_i \in \mathbb{C}$ is the complex wave speed. The real part c_r gives the dimensionless phase velocity, whereas the imaginary part c_i gives the growth rate $\omega_i = \alpha c_i$ of the wave. A stable (unstable) flow will correspond to negative (positive) values of c_i. The employment of linear theory relies on the smallness of the complex amplitude wave functions, namely $|\hat{u}(y)|$,

$|\hat{v}(y)|$, $|\hat{p}(y)| \ll 1$. The flow can be expressed in terms of the perturbed stream function $\psi = \psi_b(y) + \hat{\psi}(y)e^{i\alpha(x-ct)}$ so that

$$\hat{u} = \hat{\psi}', \qquad \hat{v} = -i\alpha\hat{\psi}. \tag{37}$$

Inserting (36) into $(10)_1$ and linearizing we obtain

$$\begin{cases} Re\Big[-i\alpha c\hat{u} + i\alpha\hat{u}u_b + u_b'\hat{v}\Big] = -i\alpha\hat{p} + i\alpha\hat{S}_{11} + \hat{S}_{12}', \\ \\ Re\Big[-i\alpha c\hat{v} + i\alpha\hat{v}u_b\Big] = -\hat{p}' + i\alpha\hat{S}_{12} + \hat{S}_{22}', \end{cases} \tag{38}$$

where $\hat{S}_{ij}(y)$ are the components of the perturbed stress and $\hat{S}_{11} + \hat{S}_{22} = 0$. On eliminating $\hat{p}$ in (38) we find

$$-Re\Big[(u_b - c)(\hat{v}'' - \alpha^2\hat{v}) - u_b''\hat{v}\Big] = 2i\alpha\hat{S}_{11}' + \hat{S}_{12}'' + \alpha^2\hat{S}_{12}, \tag{39}$$

or equivalently

$$i\alpha Re\Big[(u_b - c)(\hat{\psi}'' - \alpha^2\hat{\psi}) - u_b''\hat{\psi}\Big] = 2i\alpha\hat{S}_{11}' + \hat{S}_{12}'' + \alpha^2\hat{S}_{12}. \tag{40}$$

Now we express the components $\hat{S}_{ij}(y)$ in terms the components $\hat{D}_{ij}(y)$. From the linearization of the tensor $\mathbf{D}$

$$|\mathbf{D}| = |\mathbf{D}_b(y) + \hat{\mathbf{D}}(y)e^{i\alpha(x-ct)}| \cong |\mathbf{D}_b| + \frac{\mathbf{D}_b \cdot \hat{\mathbf{D}}}{2|\mathbf{D}_b|}e^{i\alpha(x-ct)}. \tag{41}$$

Recalling (7), (9), we write $\mathbf{S} = f(|\mathbf{D}|)\mathbf{D}$ with

$$f = f_B(\zeta) = \left[2 + \frac{B}{\zeta}\right], \qquad \text{(Bingham)}, \tag{42}$$

$$f = f_P(\zeta) = \left[2 + \frac{B\Big(1 - \exp(-\frac{2\zeta}{\epsilon})\Big)}{\zeta}\right], \qquad \text{(Papanastasiou)}. \tag{43}$$

We linearize the function $f(\zeta)$ getting

$$f\Big(|\mathbf{D}_b + \mathbf{D}e^{i\alpha(x-ct)}|\Big) \cong f(|\mathbf{D}_b|) + \frac{df}{dz}(|\mathbf{D}_b|)\frac{\mathbf{D}_b \cdot \hat{\mathbf{D}}}{2|\mathbf{D}_b|}e^{i\alpha(x-ct)}.$$

We recall that

$$|\mathbf{D}_b| = \frac{u_b'}{2}, \qquad (i\alpha\hat{u} + \hat{v}') = 0,$$

and

$$\hat{\mathbf{D}} = \begin{bmatrix} i\alpha\hat{u} & \frac{1}{2}(\hat{u}' + i\alpha\hat{v}) \\ \\ \frac{1}{2}(\hat{u}' + i\alpha\hat{v}) & \hat{v} \end{bmatrix}. \tag{44}$$

After some algebra, we find

$$\hat{S}_{11} = -\hat{S}_{22} = -f\left(\frac{u_b'}{2}\right)\hat{v}',$$

$$\hat{S}_{12} = -\frac{1}{2i\alpha}\left[f\left(\frac{u_b'}{2}\right) + \frac{u_b'}{2}\frac{df}{dz}\left(\frac{u_b'}{2}\right)\right]\left(\hat{v}'' + \alpha^2\hat{v}\right).$$

Setting

$$q(y) = f\left(\frac{u_b'}{2}\right), \qquad s(y) = \frac{1}{2}\left[f\left(\frac{u_b'}{2}\right) + \frac{u_b'}{2}\frac{df}{dz}\left(\frac{u_b'}{2}\right)\right], \tag{45}$$

we get

$$\hat{S}_{11} = \big[i\alpha q(y)\big]\hat{\psi}', \qquad \hat{S}_{22} = -\big[i\alpha q(y)\big]\hat{\psi}', \qquad \hat{S}_{12} = \big[s(y)\big]\big(\hat{\psi}'' + \alpha^2\hat{\psi}\big). \tag{46}$$

Inserting (46) into (40), we obtain the perturbation equation for $\hat{\psi}$

$$i\alpha Re\Big[(u_b - c)(\hat{\psi}'' - \alpha^2\hat{\psi}) - u_b''\hat{\psi}\Big] = -2\alpha^2\Big[q\hat{\psi}'\Big]' +$$

$$+\Big[s\big(\hat{\psi}'' + \alpha^2\hat{\psi}\big)\Big]'' + \alpha^2\Big[s\big(\hat{\psi}'' + \alpha^2\hat{\psi}\big)\Big]. \tag{47}$$

Remark 1. *When $B = 0$ (Newtonian fluid) $f = 2$ and the functions q and s are such that $q = 2$, $s = 1$. In this case equation (47) reduces to the classical Orr-Sommerfeld equation.*

Now, we turn our attention to the boundary conditions. We denote the perturbed free surface with

$$h = 1 + \hat{h}e^{i\alpha(x-ct)},$$

with $\hat{h} \in \mathbb{C}$ constant. Linearization of the kinematical boundary condition $(12)_2$ yields

$$\hat{h}(1-c) = -\hat{\psi}(1), \tag{48}$$

where we recall that $u_b(1) = 1$ because of the adopted scaling. The linearized dynamical free surface conditions $(12)_{3,4}$ become

$$\hat{h}p_b'(1) + \hat{p}(1) + \hat{S}_{11}(1) = 0, \tag{49}$$

$$\hat{h}S_{b_{12}}'(1) + \hat{S}_{12}(1) = 0. \tag{50}$$

Eliminating $\hat{h}$ from (48)-(50) we end up with

$$\begin{cases} (1-c)\dfrac{\hat{S}_{12}(1)}{S_{b_{12}}'(1)} = \hat{\psi}(1), \\ \\ \dfrac{\hat{S}_{12}(1)}{S_{b_{12}}'(1)} = \dfrac{\hat{S}_{11}(1) + \hat{p}(1)}{p_b'(1)}. \end{cases} \tag{51}$$

The pressure term $\hat{p}(1)$ in $(51)_2$ is written in terms of $\hat{\psi}$ via $(38)_1$. In particular, one can check that

$$\hat{p}(1) = 2i\alpha\hat{\psi}'(1) + \frac{\hat{\psi}'''(1) + \alpha^2\hat{\psi}'(1)}{i\alpha} - Re\hat{\psi}'(1-c). \tag{52}$$

Moreover, from (14)

$$p_b'(1) = -\xi \cot\theta, \qquad S_{b_{12}}'(1) = -\xi,$$

where ξ is given by (20) (Bingham) or by the solution of (31) (Papanastasiou). Substitution of (46), (52) into (51) provides the boundary conditions on $y = 1$ for the unknown $\hat{\psi}(y)$. The boundary conditions on $y = 0$ are $\hat{\psi}(0) = \hat{\psi}'(0) = 0$

(no-slip). In conclusion the four boundary conditions for $\hat{\psi}$ are

$$\begin{cases} \hat{\psi} = \hat{\psi}' = 0, & y = 0, \\ \hat{\psi}'' + \hat{\psi}\left[\alpha^2 - \dfrac{\xi}{s(c-1)}\right] = 0, & y = 1, \\ -is\hat{\psi}''' + \alpha\hat{\psi}'\left[i\alpha(2q - s) + Re(c-1)\right] + & \\ -\hat{\psi}\left[(\alpha s \cot\theta + is')\dfrac{\xi}{s(c-1)}\right] = 0, & y = 1. \end{cases} \tag{53}$$

Problem (47) with boundary conditions (53) is a differential eigenvalue problem for the eigenvalue c and the associated eigenfunction $\hat{\psi}$. Although the differential equation is the same as that derived in [15] for the plane Poiseuille flow, here the problem is much more complex because conditions $(53)_{2,3}$ involve the eigenvalue nonlinearly. Problem (47), (53) is homogeneous (the eigenfunction $\hat{\psi}$ is defined up to a multiplicative constant) and we must look for values of c that lead to a nontrivial solution, providing the relationship between the conditions of the primary flow and the evolution of the various disturbance modes. For fixed $(\theta, \gamma, \epsilon)$, we determine the eigenvalue $c = c(Re, \alpha)$ with maximum imaginary part denoted by c_i. The flow is stable if $c_i(Re, \alpha) < 0$ and unstable if $c_i(Re, \alpha) > 0$. The level set $c_i(Re, \alpha) = 0$ provides the neutral stability curve on the plane (Re, α). We recall that $\xi = \xi(Re, \gamma, \theta)$ in the Bingham case and $\xi = \xi(Re, \gamma, \theta, \epsilon)$ in the Papanastasiou case.

Remark 2. *When* $\alpha = 0$ (47), (53) *reduces to*

$$\begin{cases} \left[s\hat{\psi}''\right]'' = 0, & \\ \hat{\psi} = \hat{\psi}' = 0, & y = 0, \\ \hat{\psi}'' - \dfrac{\hat{\psi}\xi}{s(c-1)} = 0, & y = 1, \\ s\hat{\psi}''' + \dfrac{\hat{\psi}s'\xi}{s(c-1)} = 0, & y = 1. \end{cases} \tag{54}$$

In this case the eigenvalue problem has real coefficients meaning $c_i(0, Re) = 0$. *Therefore, the line* $\alpha = 0$ *in the* (α, Re) *plane is a neutral stability curve.*

4. Numerics

We develop a numerical procedure for solving (47), (53) based on a Galerkin method that makes use of Chebyshev polynomials of the first kind, so that we can express problem (47), (53) in terms of discretized differential operators. We choose Chebyshev polynomials since they are appropriate in describing boundary layer phenomena which are commonly encountered in flow stability problems. The physical domain $[0, 1]$ is mapped into the computational domain $[-1, 1]$ by

$$y = \frac{z+1}{2}, \qquad z = -1 + 2y \qquad\qquad \frac{d^n}{dy^n} = 2^n \frac{d^n}{dz^n}.$$

We introduce the functions

$$\phi(z) = \hat{\psi}(y), \qquad U(z) = u_b(y), \qquad q(z) = q(y), \qquad s(z) = s(y).$$

It is straightforward to see that problem (47), (53) becomes

$$i\alpha Re\Big[(U-c)\big(4\frac{d^2\phi}{dz^2} - \alpha^2\phi\big) - 4\frac{d^2U}{dz^2}\phi\Big] = -8\alpha^2\frac{d}{dz}\Big[q\frac{d\phi}{dz}\Big] +$$

$$+4\frac{d^2}{dz^2}\Big[s\big(4\frac{d^2\phi}{dz^2} + \alpha^2\phi\big)\Big] + \alpha^2\Big[s\big(4\frac{d^2\phi}{dz^2} + \alpha^2\phi\big)\Big], \tag{55}$$

$$
\begin{cases}
\phi = \dfrac{d\phi}{dz} = 0, & y = -1, \\[2ex]
4\dfrac{d^2\phi}{dz^2} + \phi\left[\alpha^2 - \dfrac{\xi}{s(c-1)}\right] = 0, & y = 1, \\[2ex]
-8is\dfrac{d^3\phi}{dz^3} + 2\alpha\dfrac{d\phi}{dz}\left[i\alpha(2q-s) + Re(c-1)\right] + & \\[2ex]
-\phi\left[\left(\alpha s\cot\theta + 2i\dfrac{ds}{dz}\right)\dfrac{\xi}{s(c-1)}\right] = 0, & y = 1.
\end{cases}
\tag{56}
$$

In the Papanastasiou case the functions $s(z)$ and $q(z)$ are given by

$$
s(z) = 1 + \frac{B}{\epsilon}\exp\left(-\frac{2}{\epsilon}\frac{dU}{dz}\right), \tag{57}
$$

$$
q(z) = 2 + B\left(\frac{dU}{dz}\right)^{-1}\left[1 - \exp\left(-\frac{2}{\epsilon}\frac{dU}{dz}\right)\right], \tag{58}
$$

while in the Bingham case

$$
s(z) = 1, \qquad q(z) = 2 + B\left(\frac{dU}{dz}\right)^{-1}. \tag{59}
$$

Equations (55)-(56) are collocated at Chebyshev-Gauss-Lobatto points

$$
z_k = \cos\left(\frac{k\pi}{N}\right), \qquad k = 0, ..., N, \tag{60}
$$

with ϕ expanded as a truncated series of Chebyshev polynomials

$$
\phi(z) = \sum_{k=0}^{N} a_k T_k(z).
$$

The problem (55)-(56) is rewritten as

$$\begin{cases} \mathcal{L}_1\phi = c\mathcal{L}_2\phi, \\ \\ \mathcal{A}_1\phi = 0, \\ \\ \mathcal{B}_1\phi = 0, \\ \\ \mathcal{M}_1\phi = c\mathcal{M}_2\phi, \\ \\ \mathcal{N}_1\phi = c\mathcal{N}_2\phi + c^2\mathcal{N}_3\phi, \end{cases} \tag{61}$$

where

$$\mathcal{L}_1 = (16s)\,\frac{d^4}{dz^4} + \left(32\frac{ds}{dz}\right)\frac{d^3}{dz^3} - \left(8\alpha^2(q-s) - 16\frac{d^2s}{dz^2} + 4i\alpha ReU\right)\frac{d^2}{dz^2} +$$

$$+\left(8\alpha^2\frac{ds}{dz} - 8\alpha^2\frac{dq}{dz}\right)\frac{d}{dz} + \left(4\alpha^2\frac{d^2s}{dz^2} + \alpha^4 s + i\alpha^3 ReU + 4i\alpha Re\frac{d^2U}{dz^2}\right), \tag{62}$$

$$\mathcal{L}_2 = (-4i\alpha Re)\,\frac{d^2}{dz^2} + i\alpha^3 Re, \tag{63}$$

$$\mathcal{A}_1 = 1, \qquad\qquad \mathcal{B}_1 = \frac{d}{dz}, \tag{64}$$

$$\mathcal{M}_1 = (4s)\frac{d^2}{dz^2} + \alpha^2 s + \xi, \qquad\qquad \mathcal{M}_2 = (4s)\frac{d^2}{dz^2} + \alpha^2 s, \tag{65}$$

$$\mathcal{N}_1 = (8s^2)\frac{d^3}{dz^3} - \left[2\alpha^2\left(2qs - s^2\right) + 2i\alpha sRe\right]\frac{d}{dz} + \left(i\alpha s\xi\cot\theta - 2\frac{ds}{dz}\xi\right), \tag{66}$$

$$\mathcal{N}_2 = (8s^2)\frac{d^3}{dz^3} - \left[2\alpha^2\left(2qs - s^2\right) + 4i\alpha sRe\right]\frac{d}{dz}, \tag{67}$$

$$\mathcal{N}_3 = (2i\alpha sRe)\frac{d}{dz}. \tag{68}$$

The function ϕ is discretized at the collocation points (60) and so the functions s, q, U. The derivative d/dz is then approximated by the Chebyshev differentiation matrix D_N defined in [8]. Hence the discretized operators (62)-(68) are $(N+1) \times (N+1)$ matrices with complex entries. We denote them with

$$\mathbf{L}_1, \quad \mathbf{L}_2, \quad \mathbf{A}_1, \quad \mathbf{B}_1, \quad \mathbf{M}_1, \quad \mathbf{M}_2, \quad \mathbf{N}_1, \quad \mathbf{N}_2, \quad \mathbf{N}_3.$$

The boundary conditions are implemented as in [18]. The discretized problem consists in a quadratic matrix eigenvalue problem of the type

$$\mathbf{P}\phi = c\mathbf{R}\phi + c^2\mathbf{W}\phi. \tag{69}$$

where

$$\mathbf{P} = \begin{bmatrix} (\mathbf{N}_1)_{0,0} & .... & (\mathbf{N}_1)_{0,N} \\ (\mathbf{M}_1)_{0,0} & .... & (\mathbf{M}_1)_{0,N} \\ (\mathbf{L}_1)_{2,0} & .... & (\mathbf{L}_1)_{2,N} \\ .... & .... & .... \\ .... & .... & .... \\ (\mathbf{L}_1)_{N-2,0} & .... & (\mathbf{L}_1)_{N-2,N} \\ (\mathbf{A}_1)_{0,0} & .... & (\mathbf{A}_1)_{0,N} \\ (\mathbf{B}_1)_{0,0} & .... & (\mathbf{B}_1)_{0,N} \end{bmatrix},$$

$$\mathbf{R} = \begin{bmatrix} (\mathbf{N}_2)_{0,0} & .... & (\mathbf{N}_2)_{0,N} \\ (\mathbf{M}_2)_{0,0} & .... & (\mathbf{M}_2)_{0,N} \\ (\mathbf{L}_2)_{2,0} & .... & (\mathbf{L}_2)_{2,N} \\ .... & .... & .... \\ .... & .... & .... \\ (\mathbf{L}_2)_{N-2,0} & .... & (\mathbf{L}_2)_{N-2,N} \\ 0 & .... & 0 \\ 0 & .... & 0 \end{bmatrix},$$

$$
\mathbf{W} = \begin{bmatrix} (\mathbf{N}_3)_{0,0} & .... & (\mathbf{N}_3)_{0,N} \\ 0 & .... & 0 \\ .... & .... & .... \\ .... & .... & .... \\ 0 & .... & 0 \end{bmatrix}.
$$

Problem (69) is finally transformed in the linear generalized eigenvalue problem

$$
\begin{bmatrix} \mathbf{P} & \mathbf{0} \\ & \\ \mathbf{0} & \mathbf{I} \end{bmatrix} \begin{bmatrix} \phi \\ \\ c\phi \end{bmatrix} = c \begin{bmatrix} \mathbf{R} & \mathbf{W} \\ & \\ \mathbf{I} & \mathbf{0} \end{bmatrix} \begin{bmatrix} \phi \\ \\ c\phi \end{bmatrix}, \tag{70}
$$

where $\mathbf{0}$, $\mathbf{I}$ are the $(N+1) \times (N+1)$ null and identity matrix respectively. The problem (70), which is equivalent to (69), is twice as large as (69). The system is solved in the Matlab environment by means of QZ decomposition. We observe that, for "large" N, the round-off errors begin to accumulate, so one must be careful in the selection of the proper N. To maintain high accuracy we have used (69) with a small value of N to determine a good approximation of c and then we have improved such a value through the Newton-QR inverse iteration method described in [17] to determine the eigenvalue c with good accuracy.

5. Results

It is well known that in the Newtonian case there are two types of modes that govern the stability of the flow down an incline, namely the surface (or soft) mode and the shear (or hard) mode, see [10], [12], [9], [5], [6]. The surface mode is essentially a surface wave slightly modified by viscosity, whereas the shear mode is a Tollmien-Schlichting shear wave modified by the presence of a free surface, see [22]. The surface mode is related to the formation of waves on the free surface, while the shear mode is related to internal shear of layers within the fluid. The dominant mode is established by the tilt angle of the inclined plane. For "small" values of θ shear modes are dominant, while in the opposite case the surface modes govern instability. The instability effects of the shear mode begin to appear at small angles and are characterized by critical Reynolds of the order of thousands, as in plane Poiseuille flow. For larger values of θ instability is driven by surface modes, with the critical Reynolds number being a decreasing function of θ. This is physically consistent, as one expects that the increase of the inclination angle tends to destabilize the flow. The critical Reynolds of the surface modes is generally smaller than that of the shear modes, but for sufficiently small angles the opposite is true, see Fig. 8. In the latter case the flow is essentially horizontal and the flow is comparable to a plane Poiseuille flow with a free surface (open channel).

In most of the papers dealing with stability down an incline particular attention is paid to the so-called "long-wave approximation", which consists in a perturbation method aimed at determining the neutral stability curves for small wave numbers. The perturbation method consists in expanding the eigenvalue and the eigenfunction in power series of α and studying the relative eigenvalue problem at the various degrees of approximation assuming that α is "small". Here we will not consider this type of asymptotic analysis and we will solve the general problem only numerically. We refer the reader to [4] where this asymptotic analysis is performed.

We shall see that when considering the Bingham model the flow is essentially that of a fluid flowing between rigid surfaces (indeed the yield surface cannot be perturbed) but with a monotonically increasing basic profile. We will prove that the Bingham flow is unconditionally linearly stable for every Reynolds number, in agreement with the results of [11]. In the Papanastasiou case we shall see that the flow can become unstable with the critical Reynolds being a decreasing function of the yield stress parameter γ and of the tilt angle θ. We will also see that the wave speed of the neutral surface mode is a decreasing function of the Reynolds number and that, for fixed Re, the corresponding neutral mode has a wave velocity that decreases with γ and θ. The decrease of the surface speed with θ is also observed in the Newtonian case, see Fig. 4 of [9]. Finally, we shall see that the presence of the yield stress prevents the occurrence of shear modes.

5.1. *Newtonian fluid*

We begin our discussion by testing the numerical code for a Newtonian fluid, i.e. when $B = 0$ (or $\epsilon = \infty$). This allows us to validate the efficiency and correctness of our numerical code. In the Newtonian case $\xi = 2$, $s = 1$, $q = 2$ and

$$u_b(y) = y(2-y), \qquad U(z) = \frac{(z+1)(3-z)}{4}. \tag{71}$$

This problem has been extensively studied, see [24], [19], [10], [12] [5], [6] and we can compare the results of these papers with the ones obtained here setting $B = 0$. To this aim we must pay attention to the Reynolds number which is often not univocally defined. For instance in [24] the problem is solved via perturbation technique limited to long waves (surface modes) obtaining the famous relation for the critical Reynolds

$$Re_c = \frac{5}{6}\cot\theta, \tag{72}$$

which holds in the absence of surface tension. Due to the different scaling, here the critical Reynolds predicted by the perturbation method must be corrected by a factor 3/2, namely

$$Re_c = \frac{5}{4}\cot\theta. \tag{73}$$

The critical condition (73) provides the linear approximation (or long-wave approximation) of the neutral curve $c_i(Re, \alpha) = 0$ for small values of α. It is a straight vertical line in the (Re, α) plane that is tangent to the neutral curve in $\alpha = 0$. Notice that, in view of Remark 2, the point $(Re_c, 0)$ is a bifurcation point of the neutral stability curve. In Fig. 7 we display the neutral stability curves for a Newtonian fluid flowing down an inclined plane for $\theta = 4^o, 8^o, 15^o, 45^o$. Within this range of tilt angles instability is governed by surface modes. The stability region is placed to the left of the neutral curve, while the instability region is placed to the right. The dashed lines indicate the critical Reynolds number evaluated by the asymptotic expansion at the first order, that is using equation (73). The dashed lines represent therefore the first order Taylor approximation of the curve $c_i(Re, \alpha) = 0$ around $\alpha = 0$. The agreement between Re_c evaluated numerically and Re_c evaluated from (73) is excellent.

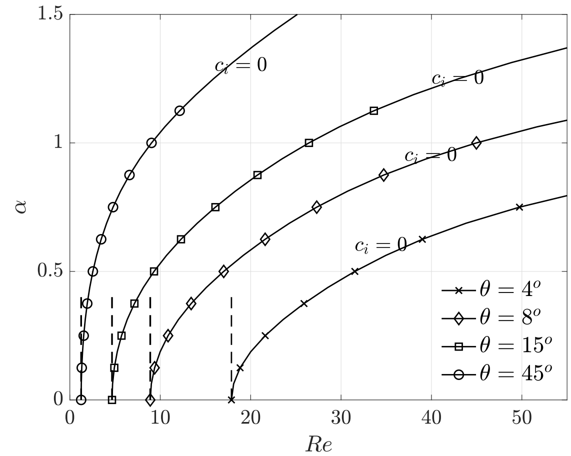

Figure 7: Neutral stability curves for a Newtonian fluid at different inclination angles with no surface tension. The dashed vertical lines identify the critical Reynolds number determined by long-wave approximation, i.e. (73). Notice that the fluid is less stable as θ is increased.

In Fig. 8 we show the neutral stability curve for small values of the tilt angle θ. We begin with $\theta = 18'$ for which (73) predicts a $Re_c = 238.73$. As the angle θ is reduced shear modes start to appear in the form of a protuberance of the neutral curve, which becomes more pronounced as θ tends to zero. The critical Re_c of the surface mode is given by the intersection of the neutral curve with the Re axis, while the critical Reynolds of the shear mode is given by the peak of the protuberance. For a tilt angle approximately larger than $\approx 2'$ the critical Reynolds of the surface mode is smaller than that of the shear mode. For smaller values of θ the situation is reversed with Re_c of the shear mode being smaller than that of the surface mode. In the latter case the shear mode becomes the primary source of instability. As observed in [10], the Re_c of the surface mode is monotonically decreasing with θ whereas the Re_c of the shear mode is non monotonic.

5.2. Bingham fluid

In this section we study the linear stability of the Bingham flow. Let us denote by $\sigma + \hat{\sigma}e^{i\alpha(x-ct)}$ the perturbed yield surface, where σ is given by (19)

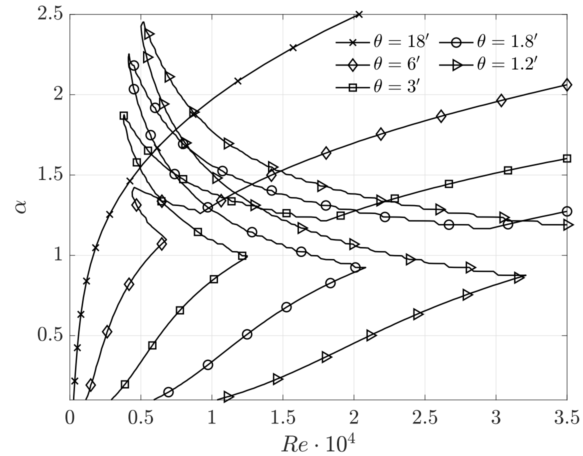

Figure 8: Neutral stability curves for a Newtonian fluid for "very small values" of the inclination angle θ. The protuberance on the neutral curve marks the transition to instability due to the shear modes.

and $\hat{\sigma}$ is a complex constant. In the Bingham flow the unyielded part of the fluid layer behaves as a rigid solid and thus cannot be deformed. Following [2], [15], [11] we know that inside the intact plug the disturbance has no effects implying $\hat{\sigma} = 0$. This means that the yield surface essentially acts as a rigid wall bounding the sheared layer. In other words, the linear stability problem is that of a plane Poiseuille motion in which the flow is driven by gravity and by the motion of the upper surface. As a consequence, instability can be only shear-driven and there are no surface modes associated with the free surface. The upper boundary condition for the perturbed stream function is

$$\hat{\psi}(\sigma) = \hat{\psi}'(\sigma) = 0.$$

The functions $s(y)$, $q(y)$ are

$$s(y) = 1, \qquad q(y) = 2\left(1 + \frac{B}{u_B'}\right),$$

while the basic velocity $u_B(y)$ is the one defined in (21). Substituting these functions into (47) and applying the spatial transformation

$$z = -1 + \frac{2}{\sigma}y \qquad \Longleftrightarrow \qquad y = \frac{\sigma}{2}(z+1) \qquad \Longrightarrow \qquad \frac{d^n}{dy^n} = \left(\frac{2}{\sigma}^n\right)\frac{d^n}{dz^n},$$

that maps the phyiscal domain $[0,\sigma]$ into the computational domain $[-1,1]$ we end up with the following eigenvalue problem

$$i\alpha Re\left[(U-c)\left(\frac{4}{\sigma^2}\frac{d^2\phi}{dz^2}-\alpha^2\phi\right)+\frac{2}{\sigma^2}\phi\right]=$$

$$-\frac{16\alpha^2}{\sigma^2}\frac{d}{dz}\left[\left(1+\frac{B\sigma}{(1-z)}\right)\frac{d\phi}{dz}\right]+$$

$$+\frac{4}{\sigma^2}\frac{d^2}{dz^2}\left[\frac{4}{\sigma^2}\frac{d^2\phi}{dz^2}+\alpha^2\phi\right]+\alpha^2\left[\frac{4}{\sigma^2}\frac{d^2\phi}{dz^2}+\alpha^2\phi\right], \tag{74}$$

$$\phi(\pm 1)=\frac{d\phi}{dz}(\pm 1)=0, \tag{75}$$

where

$$\hat{\psi}(y)=\phi(z), \qquad u_B(y)=U(z)=1-\left(1-\frac{z+1}{2}\right)^2,$$

and where $B=B(Re,\Gamma)$ is provided by (23). The problem (74) is again discretized through spectral collocation and solved numerically. Consistently with the results of [2], [11], we find that the linear perturbations are always stable, i.e., $c_i(Re,\alpha)<0$, for any Reynolds number and for any Γ. In Fig. 9 we show the maximum of the imaginary part c_i of the spectrum for $\Gamma=1,8,20$. As one can see this function is decreasing with Γ showing that the increase of the yield stress has a stabilizing effect on the basic flow. It is also evident that, for $Re\to 0$, the function c_i tends to $-\infty$.

5.3. *Papanastasiou fluid*

Here we present the results for the Papanastasiou fluid. We begin by noticing that

$$s(y)=1+\frac{Be^{-\frac{u_b'}{\epsilon}}}{\epsilon}, \qquad q(y)=2+\frac{2B(1-e^{-\frac{u_b'}{\epsilon}})}{u_b'},$$

and

$$s(z)=1+\frac{Be^{-\frac{2}{\epsilon}\frac{dU}{dz}}}{\epsilon}, \qquad q(z)=2+\frac{B\left(1-e^{-\frac{2}{\epsilon}\frac{dU}{dz}}\right)}{\frac{dU}{dz}}. \tag{76}$$

The velocity of the basic flow is given by (32). Inserting the functions (76) in the eigenvalue problem (61) we solve the discretized problem (69).

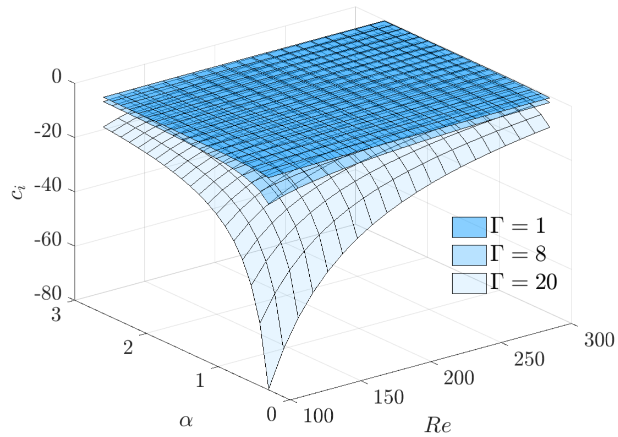

Figure 9: Maximum of the imaginary part c_i of the spectrum for $\Gamma = 1, 8, 20$.

In Fig. 10, 11 we show the neutral stability curves for increasing values of γ with $\theta = 5^o$ and $\theta = 10^o$. The critical Reynolds number is a decreasing function of γ, showing that the increase of the yield stress has a destabilizing effect on the flow. As expected, the flow becomes less stable when the tilt angle is increased. The curves with $\gamma = 0$ correspond to the Newtonian case. The parameter ϵ is taken as $\epsilon = 0.1$. This choice is dictated by the fact that for the typical values of $\gamma \in [10^{-2}, 1]$ it is sufficient to take $\epsilon = 0.1$ to have $E_R \leqslant 1\%$.

In Fig. 12 we show the neutral stability curves for $\gamma = 0.1$ at angles $\theta = 3^o, 6^o, 9^o, 12^o, 15^o$. It is evident that Re_c is decreasing with θ, as physically expected. In Fig. 13 we show the wave velocity of various neutral curves at different angles. The wave speed increases as θ decreases, a type of behavior also encountered in the Newtonian case, see [9]. The wave velocity is always greater than the surface velocity of the basic flow. For large values of Re the wave velocity asymptotically approaches the surface velocity and, as in the Newtonian case, there are no critical layers where wave speed equals fluid speed.

In Fig. 14 we show the wave speed for various γ at $\theta = 15^o$. We notice that the variation of γ has little effect on the wave speed. Finally in Fig. 15, 16 we plot

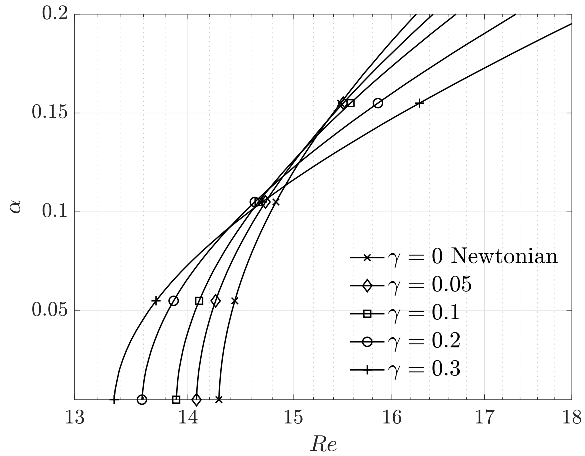

Figure 10: Neutral curves for $\gamma = 0,\ 0.05,\ 0.1,\ 0.2,\ 0.3,\ 0.4$ with $\theta = 5^o$.

the critical Reynolds as a function of γ and θ respectively. It is evident that the dependence of Re_c on θ is nonlinear with the critical Reynolds approaching zero when $\theta \to \pi/2$. In Fig. 15 we show the critical Reynolds number as a function of γ for different values of θ. We observe that Re_c is a decreasing function of γ, proving that the increase of the yield stress has a destabilizing effect on the flow.

6. Conclusions

In this paper we have investigated the linear stability of the unidirectional steady flow of a fluid (Papanastasiou) whose response mimics that of a Bingham fluid. The geometrical setting is that of a free surface flow down an inclined plane. The main advantage of using a regularized model is that we avoid all the issues related to the presence of truly unyielded zones. Indeed, in the regularized model the stress is defined everywhere in the fluid domain and not only in the yielded part.

We have proved that while the Bingham flow is unconditionally stable for every Re, the Papanastasiou flow can become unstable if Re is larger than a critical threshold that depends on the rheological parameters and on the tilt

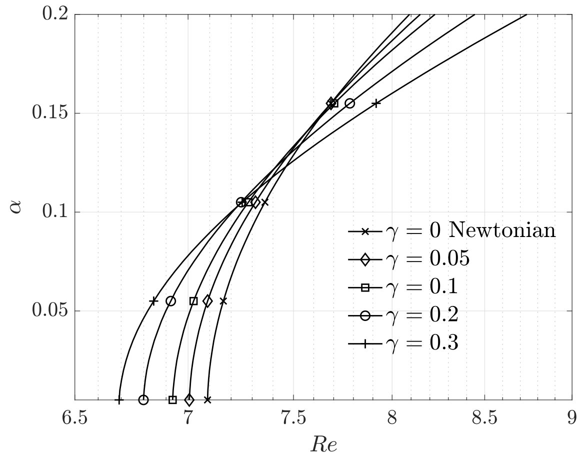

Figure 11: Neutral curves for $\gamma = 0,\ 0.05,\ 0.1,\ 0.2,\ 0.3,\ 0.4$ with $\theta = 10^o$.

angle, no matter how good the approximation is. In other words, we have shown that even if the basic Papanastasiou flow is almost indistinguishable from the classical Bingham flow, their stability properties can be different. This peculiarity was already observed for plane Poiseuille flow [15].

Moreover, we have shown that, contrary to what occurs in channel flows, the presence of the yield stress leads to critical Reynolds that are smaller than those of the Newtonian fluid, showing that in free surface flows down an incline the yield stress has a destabilizing effect.

Acknowledgements

This research was partially supported by GNFM of Italian INDAM.

References

[1] Astarita, G., The engineering reality of the yield stress. Journal of Rheology, 34(2), (1990), 275-277.

[2] Balmforth N.J., Liu J.J., Roll waves in mud, J. Fluid Mech., 519, (2004), 33–54.

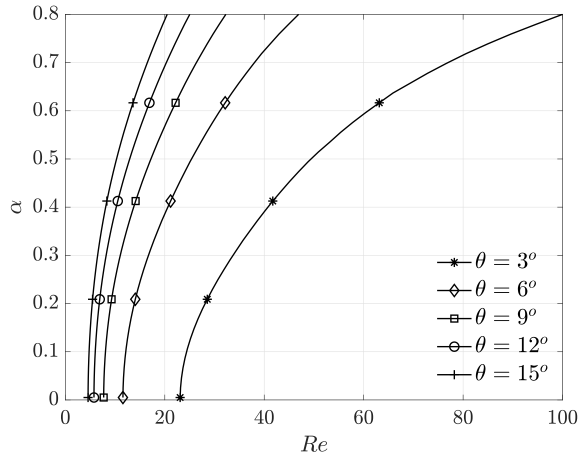

Figure 12: Neutral curves for angles $\theta = 3^o, 6^o, 9^o, 12^o, 15^o$ with $\gamma = 0.1$.

[3] Barnes H.A., Walters K., The yield stress myth?, Rheologica Acta, 24,(1985) 323–326.

[4] Calusi B., Farina A., Fusi L., Rosso F., Long-wave instability of a regularized Bingham flow down an incline, submitted.

[5] Benjamin T.B., Wave formation in laminar flow down an inclined plane, J. Fluid Mech., 2, (1957), 554-574.

[6] Benney D.J., Long waves on liquid films, J. Math. and Physics, 45, (1966), 150–155.

[7] Bercovier M., Engleman M., A finite-element method for incompressible non-Newtonian flows, J. Comp. Phys., 36, (1980), 313-326.

[8] Canuto, C., Hussaini, M. Y., Quarteroni, A., Zang, T.A., (1987). Spectral methods in fluid dynamics. Springer-Verlag, New York.

[9] Chin, R.W., Abernath F.H., Bertschy J.R., Gravity and shear wave stability of free surface flows. Part 1. Numerical calculations, Journal of Fluid Mechanics, 168, (1986), 501–513.

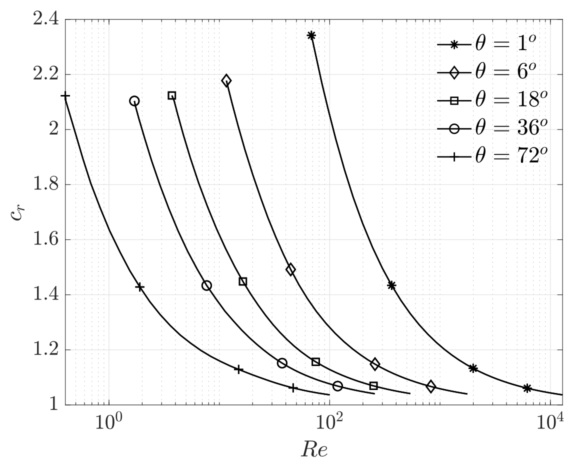

Figure 13: Wave velocity of the neutral mode for angles $\theta = 1^o, 6^o, 18^o, 36^o, 72^o$ with $\gamma = 0.1$.

[10] De Bruin, G. J. Stability of a layer of liquid flowing down an inclined plane, Journal of Engineering Mathematics, 8(3), (1974), 259-270.

[11] Falsaperla P., Giacobbe A., Mulone G., Stability of the Plane Bingham–Poiseuille Flow in an Inclined Channel, Fluids, 5, (2020), 141.

[12] Floryan, J. M., Davis, S. H., Kelly, R. E. Instabilities of a liquid film flowing down a slightly inclined plane. The Physics of fluids, 30(4), (1987), 983-989.

[13] Frigaard I.A., Nouar C., On the usage of viscosity regularisation methods for visco-plastic fluid flow computation, J. Non-Newtonian Fluid Mech., 127 (2005), 1–26.

[14] I.A. Frigaard, Paso K.G., de Souza Mendes P.R., Bingham's model in the oil and gas industry, Rheologica Acta, 56, (2017), 259–282.

[15] Fusi, L., Farina, A., Rajagopal, K. R., Vergori, L. (2022). Channel flows of shear-thinning fluids that mimic the mechanical response of a Bingham fluid. International Journal of Non-Linear Mechanics, 138, 103847.

[16] Glowinski R., Lions J.L., Tremolieres R., Analyse Numérique des inequa-

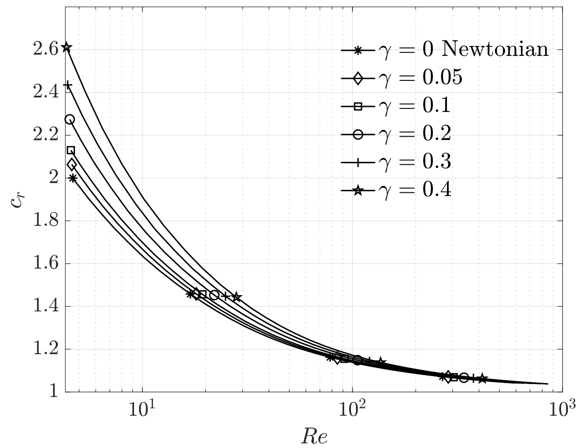

Figure 14: Wave velocity of the neutral mode for $\gamma = 0,\ 0.05,\ 0.1,\ 0.2,\ 0.3,\ 0.4$ with $\theta = 15^o$.

tions variationelles, vol. 2, Dunod, Paris, 1976 (English trans. Numerical Analysis of Variational Inequalities, North-Holland, Amsterdam, 1981).

[17] Güttel S., Tisseur F., The nonlinear eigenvalue problem, Acta Numerica, 26, (2017), 1–94.

[18] Horng, A.T.L., Chebyshev collocation method on solving stability of a liquid layer flowing down an inclined plane, The Mechanics of Thin Film Coatings. (1996), 95-106.

[19] Lin, S.P., Instability of a liquid film flowing down an inclined plane, The Physics of Fluids, 10(2), (1967), 308-313.

[20] Liu K. F., Mei C. C., Slow spreading of a sheet of Bingham fluid on an inclined plane. Journal of fluid mechanics, 207, (1989) 505-529.

[21] Papanastasiou T.C., Flows of materials with yield, J. Rheol. 31 (5) (1987) 385–404.

[22] Schmid P. J., Henningson D. S., Jankowski D. F., Stability and transition in shear flows. applied mathematical sciences, Appl. Mech. Rev., 142, 55(3), (2002).

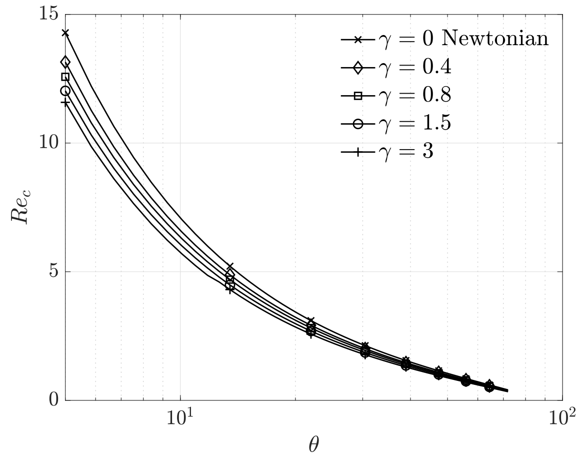

Figure 15: Critical Reynolds as a function of θ for various γ.

[23] Wu Y. H., Liu K. F., Formulas for calibration of rheological parameters of bingham fluid in couette rheometer, Journal of Fluids Engineering, 137(4), (2015).

[24] Yih C.S., Stability of liquid flow down an inclined plane, The Physics of Fluids, 6, 321, (1963), 321-334.

[25] You Z., Huilgol R. R., Mitsoulis E. Application of the Lambert W function to steady shearing flows of the Papanastasiou model, International journal of engineering science, 46(8), (2008), 799-808.

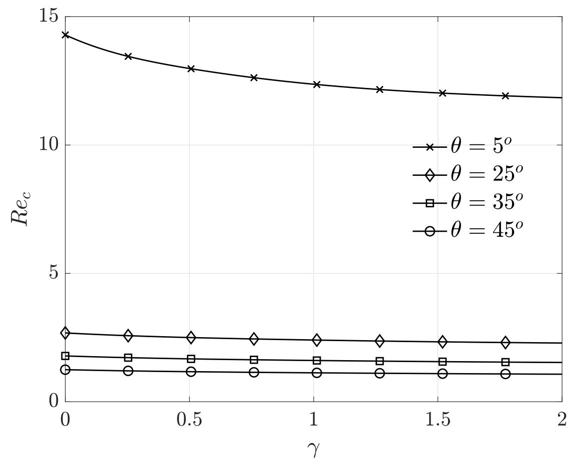

Figure 16: Critical Reynolds as a function of γ for various θ.